LAWRENCE
LIVERMORE
NATIONAL
LABORATORY

LLNL-JRNL-407615

Determining Orientational Structure of Diamondoid Thiols Attached to Silver Using Near Edge X-ray Absorption Fine Structure Spectroscopy

T. M. Willey, J. R. I. Lee, J. D. Fabbri, D. Wang, M. Nielsen, J. C. Randel, P. R. Schreiner, A. A. Fokin, B. A. Tkachenko, N. A. Fokina, J. E. P. Dahl, R. M. K. Carlson, L. J. Terminello, N. A. Melosh, T. van Buuren

October 8, 2008

Journal of Electron Spectroscopy and Related Phenomena

Disclaimer

Determining Orientational Structure of Diamondoid Thiols Attached to Silver Using Near Edge X-ray Absorption Fine Structure Spectroscopy

Trevor M. Willey[1*], Jonathan R. I. Lee[1], Jason D. Fabbri[2], Dongbo Wang[3], Michael H. Nielsen[4], Jason C. Randel[2], Peter R. Schreiner[5], Andrey A. Fokin[5], Boryslav A. Tkachenko[5], Natalie A. Fokina[5], Jeremy E. P. Dahl[6], Robert M. K. Carlson[6], Louis J. Terminello[1], Nicholas A. Melosh[2], and Tony van Buuren[1]

1) Lawrence Livermore National Laboratory, 7000 East Avenue, Livermore CA 94550
2) Stanford University, 476 Lomita Mall, Stanford, CA 94305
3) Department of Geosciences, Virginia Tech, Blacksburg, VA 24061
4) University of California, Davis, CA 95616
5) Institute of Organic Chemistry, Justus-Liebig University Giessen, Heinrich-Buff-Ring 58, 35392 Giessen, Germany
6) MolecularDiamond Technologies, Chevron Technology Ventures, 100 Chevron Way, Richmond, CA 94802

* e-mail address: willey1@llnl.gov

Keywords:
NEXAFS; Self-assembled monolayers; diamondoids; thiols; molecular electronics; nanodiamond.

LLNL-JRNL-407615

Abstract

Near-edge x-ray absorption fine structure spectroscopy (NEXAFS) is a powerful tool for determination of molecular orientation in self-assembled monolayers and other surface-attached molecules. A general framework for using NEXAFS to simultaneously determine molecular tilt and twist of rigid molecules attached to surfaces is presented. This framework is applied to self-assembled monolayers of higher diamondoids, hydrocarbon molecules with cubic-diamond-cage structures. Diamondoid monolayers chemisorbed on metal substrates are known to exhibit interesting electronic and surface properties. This work compares molecular orientation in monolayers prepared on silver substrates using two different thiol positional isomers of [121]tetramantane, and thiols derived from two different pentamantane structural isomers, [1212]pentamantane and [1(2,3)4]pentamantane. The observed differences in monolayer structure demonstrate the utility and limitations of NEXAFS spectroscopy and the framework. The results also demonstrate the ability to control diamondoid assembly, in particular the molecular orientational structure, providing a flexible platform for the modification of surface properties with this exciting new class of nanodiamond materials.

Introduction

Near-edge x-ray absorption fine structure (NEXAFS) spectroscopy is a powerful tool to determine molecular orientation of self-assembled monolayers (SAMs). Typically, molecular orientation is derived using a set of transition dipole moments in a plane or along a specific vector direction to determine a single parameter, usually the polar angle of the molecules[1]. Many systems, however, consist of atomic environments with transition dipole moments in various directions and require more than one parameter to define orientation. Often, two parameters such as a polar (tilt) and a dihedral (twist) angle are sufficient to describe molecular orientation. For example, recently, additional functional groups attached to the end of aromatic SAMs were used to elegantly simultaneously determine both tilt and twist[2]. In this work, the orientation of diamondoid thiolate SAMs are derived from the NEXAFS using a more generalized framework, allowing for arbitrary choice of molecular axis and arbitrary molecule structure. At the core of the framework, all possible tilts and twists consistent with the angular-dependent NEXAFS are compared with all sterically possible orientations. The overlap between these two give all possible orientations within the accuracy and limitations of the approximation used to model the transition dipole moments. The approximate but venerable "building-block" model[1, 3-5] is primarily used here in the tilt-twist framework to approximate transition dipole moments. We have used elements and variants of this framework in various SAM systems[6-9](including supporting online information), and in this paper, we will describe the details of the method to determine the orientation of diamondoid thiols on silver surfaces.

Diamondoids are hydrocarbon molecules with cubic-diamond-cage structures that have unique properties with potential value for nanotechnology. The lower diamondoids, with three or fewer diamond cages, are adamantane, diamantane, and triamantane. Higher diamondoids, nanometer-sized diamond molecules with greater than three diamond cages, have largely evaded laboratory synthesis[10] and have only recently been purified from petroleum sources[11]. These higher diamondoids exhibit constitutional isomerism, or multiple structural forms for the same number of cages. For example, the four tetramantane isomers, two of which are enantiomers, resemble the structures of a rod, left- and right- handed helices, and a trigonal platform. As the number of diamond cages increases, multiple molecular weights become possible within the same family and the numbers of structural isomers greatly expands. In contrast to larger diamond nanoparticles (~2.5 nm), monodispersed diamondoids can be isolated in high purity and with isomeric selectivity[11]. The combination of a wide range of structures, high purity, and selective functionalization[10] makes diamondoids an ideal platform for studies of self-assembly with various tunable parameters such as the diamondoid size, shape, and thiol substitution position[12].

Diamondoid electronic properties are an interesting blend between macroscopic diamond and nanoscale sp^3-bonded hydrocarbon molecules[13-16]. In contrast to other group IV nanoparticles, diamondoids exhibit HOMO-LUMO gap tunability, primarily through changes in the occupied states[13, 17-23]. Negative electron affinity has been predicted[21], and demonstrated[7] through the highly monochromatic emission by [121]tetramantane-6-thiol (**2**, Figure 1) on Au and Ag surfaces. In this case, the transfer of electrons from the metal to the diamondoid, electron-phonon scattering, and negative electron affinity all play key roles in the emission process[7, 24, 25].

In order to take advantage of the unique properties that diamondoids offer, robust processing and handling techniques must be developed. Over the past two decades, SAMs of thiol-functionalized molecules on Au, Ag, and other noble metals have emerged as one of the most convenient and widely used means for forming well-ordered films of small molecules[26]. Self-assembled monolayers of adamantane-1-thiol, the smallest, most abundant, and most readily synthesized diamondoid, have been

extensively studied for nanolithography applications with low defect densities[27-29] and facile displacement by alkane thiols[28-31].

With the recent success of site-specific functionalization of diamondoids[10, 12, 32-35], it is now possible to use higher diamondoids as molecular building blocks to yield materials with well-defined structures, including SAMs of higher diamondoids. A recent study of eight diamondoid thiol SAMs on gold substrates with sizes up to four cages demonstrated tunability of both the geometrical and electronic structure of the diamondoid monolayers[6].

In this paper, SAMs formed from four higher diamondoid thiols on silver are investigated using near-edge x-ray absorption fine structure spectroscopy to determine the molecular orientation of the diamondoids on the surface. The four diamondoid thiols demonstrate how the substitution position of the thiol moiety and the choice of diamondoid carbon-framework structure affect diamondoid orientation and the ability of NEXAFS to determine this orientation. Two [121]tetramantane thiols are investigated by combining the NEXAFS results with the sterically allowable tilt and twist angles. These demonstrate the ability to control diamondoid orientation through the position of the thiol. Two structural isomers, the rod-like [1212]pentamantane and pyramid-shaped [1(2,3)4]pentamantane, demonstrate the ability and limitations of NEXAFS to determine orientation. These results, combined with forthcoming complementary measurements (e.g., STM) will provide a comprehensive characterization of diamondoid monolayers formed through self-assembly on silver and other substrates.

Experimental

Diamondoids were extracted and purified from petroleum sources[11], and the respective thiols **1**–**4** (Fig. 1) were prepared as described previously[10, 12, 32-35]. Silver substrates were prepared by evaporating 5nm Ti onto Si(100) wafers followed by 50 to 100 nm silver. The substrates were stored in vacuum until immersion in solutions. Monolayers from structures **1**, **2**, and **4** were formed via ~ 1 mM ethanolic solutions from ~12 to ~48 hours. The addition of 10 vol% of toluene prior to dilution in ethanol and/or mild heating (~30° C) was necessary to aid in dissolving the thiols. The monolayer based on structure **3** was formed in toluene. After removal from the diamondoid thiol solutions, samples were rinsed with clean solvent, carefully dried with nitrogen, and quickly loaded into the vacuum chamber where they were held under ultra-high vacuum (UHV) environment below ~ 10^{-9} torr to minimize exposure to ambient laboratory conditions[36].

X-ray absorption and photoelectron spectra were recorded on beamline (BL) 8.2 of the Stanford Synchrotron Radiation Lightsource (SSRL, SPEARIII) at the Stanford Linear Accelerator Center(SLAC)[37, 38]. The cross-section of the focused beam was approximately 1 mm in diameter. XPS spectra were acquired on all monolayers subsequent to NEXAFS; S 2p photoelectron spectra were acquired with 270 eV incident photons (just below the carbon K-edge) and C 1s were acquired at 500 eV, at a take-off angle of 70°. C 1s intensities were consistent with monolayer coverage, and a prominent doublet with S $2p_{3/2}$ at about 161.9 eV, characteristic of silver-thiolate bonding, indicated chemisorbed monolayers with no more than monolayer coverage[39]. Sample 2, however, also possessed a significant doublet at about 161 eV which is most commonly, but not exclusively, attributed to elemental sulfur on the surface[39].

NEXAFS spectra were recorded simultaneously in both total electron yield (TEY) and Auger electron yield (AEY) modes; TEY are presented and used in this work. All NEXAFS signals were normalized to the I_0 current, which was recorded for the incident x-ray beam via an Au grid located

upstream of the experimental sample. To ensure minimal effect on the I_0 signal from predominantly organic contaminants absorbed on the surface of the grid, it was frequently coated with a fresh layer of evaporated Au. The TEY response differs for Au and Ag, and as a consequence, double normalization is needed to deconvolute the carbon signal from artifacts caused by beamline and substrate. Following measurement of the C *K*-edge NEXAFS of a diamondoid thiol SAM on Ag, a reference SAM and/or the monolayer sample was gently heated in UHV until the C 1s peak was no longer visible in the photoelectron spectrum. This process removes the carbonaceous SAM and leaves a sufficiently clean Ag reference substrate[39]. The normalized TEY signal for SAMs on Ag is thus:

Equation 1

$$TEY_{Ag} = \frac{I_s}{I_{0,s}} \cdot \frac{I_{0,Ag}}{I_{Ag}}$$

where I_s is the sample current and I_{Ag} is the current from the clean Ag surface; $I_{0,s}$ and $I_{0,Ag}$ are the respective concurrently acquired I_0 currents.

The π* resonance intensity in NEXAFS from freshly-cleaved highly oriented pyrolytic graphite (HOPG) served both as an energy calibration standard and as a measure of the degree of linear polarization, *P*, of the incident beam. HOPG incident angles were carefully selected such that comparison of the C *K*-edge π* resonance intensity yielded the relative magnitudes of E_p^2 and E_s^2, where E_p and E_s represent the electric field in-plane and perpendicular to the plane of incidence respectively. *P* was then calculated according to:[1, 40]

Equation 2

$$P = \frac{E_p^{\,2}}{E_p^{\,2} + E_s^{\,2}}$$

The calculated polarization was 99% in the plane of the storage ring. Care was taken to ensure that the effects of beam damage on the samples were minimized when conducting the measurements. Each spectrum was recorded from a fresh region of the sample surface and beam exposure during data collection was limited to the timeframe required for good signal to noise statistics.

Analysis

NEXAFS yields a quantitative determination of molecular orientation for rigid structures such as the diamondoids. The intensity of a NEXAFS resonance is proportional to the dot product of the electric field vector in the x-ray beam and the transition dipole moment for the unoccupied orbital into which the core electron is promoted. By rotating the sample, one can vary the electric field to be completely in the surface plane at normal beam incidence, and nearly normal to the surface at grazing incidence. Analysis of NEXAFS resonance intensity as a function of incidence angle leads to the determination of molecular orientation.

Diamondoids present significant challenges to using a standard NEXAFS analysis. The diamondoids are highly symmetrical structures, and therefore, one single resonance with one TDM, or one single set of resonances with TDMs in a particular plane cannot be used to determine molecular orientation. As will be shown, the NEXAFS spectra of many diamondoid thiolates on Ag exhibit small but reproducible angular dependence, which with the appropriate analysis, can yield a quantitative assignment of diamondoid orientation within the SAMs. Determining diamondoid orientation necessitated the development of a general framework and requires modeling of TDMs. For simplicity and transparency, we are using the crude but venerable "building block" approach, where electronic transitions from the C 1s into C-H σ* / R* and C-C σ* are used; the transition dipoles are modeled as coincident with the axes of the C–H bonds and C–C bonds.

This approximation is perhaps the most simple and widely used to determine molecular orientation[1], but it is also important to understand its limitations. For example, the assumption that C-C and C-H σ* are dipoles coincident with the bonds can fail for extended alkanes where the angular dependencies of the C-C σ* transition dipoles are more accurately described as directed along the backbone of the hydrocarbon[4, 5], but even a molecular orbital approach can lack accuracy[3]. Computed x-ray absorption[41-44] is useful to understand how these various complex phenomena affect angular dependent resonances in alkanes and other molecules on surfaces; ultimately, this will also be the most accurate method for determining transition dipole moments. Here, the building block scheme is employed because of its simplicity, and in contrast to examples above, unlike extended alkanes, diamondoids are compact, rigid structures where the "building block" scheme provides a suitable means to obtain an approximate orientation of the diamondoids that is more quantitative than simple inspection of the NEXAFS. Further, preliminary DFT calculations confirm that TDMs obtained from the building block are sufficiently similar to computed TDMs[39] for diamondoids investigated in this work.

A molecular tilt and a molecular twist angle describe the orientation of a surface-attached diamondoid (figure 1). These parameters are defined with respect to a conveniently defined molecular axis. The first parameter, the tilt (also known as polar or colatitudal) angle α of the diamondoid is measured with respect to the surface normal. The second parameter, the twist (or dihedral) angle β describes the degree of rotation about the molecular axis. The third parameter, azimuthal angle ϕ, is important to systems which exhibit less than three-fold symmetry at the surface[1]. On gold or silver substrates, however, the azimuthal angle can be averaged and decoupled from the colatitudal and dihedral angles due to the (nominally) threefold symmetry of the underlying substrate and the fact that the cross-sectional area of the incident x-ray beam (~1 mm^2) vastly exceeds the average domain size. Although the azimuthal angle does not play a role in determining orientation, one cannot independently resolve tilt and twist angles from the NEXAFS data as acquired in this study. It is possible, however, to derive a manifold of all combinations of tilt and twist that are consistent with the angular dependence of the NEXAFS and are also sterically viable.

A NEXAFS resonance has intensity that can be written as the sum of the dot products squared of TDMs with the electric field of the incident radiation:[1]

Equation 3

$$I = K \cdot \sum_i \left(\mathbf{E} \cdot \mathbf{O}_i \right)^2$$

In this equation, I is the intensity of the resonance, **E** is the electric field, and the $\mathbf{O_i}$ are the transition dipole moments (TDMs) of resonaces of interest, each having a peak in the NEXAFS centered at a particular energy, and K is a proportionality constant that incorporates several scaling factors including the transition cross-section and the detection efficiency. The electric field **E** can be represented in terms of the polarization P (Equation 2), and the incident angle θ of the x-rays where θ=90° is incident normal to the surface.

The TDMs are defined with respect to an arbitrary molecular axis selected for the system of study. Two types of convenient molecular axes are chosen for each SAM studied in this work. The first is along the long axis of the [121]tetramantane and [1212]pentamantane and corresponds to a [110] diamond lattice direction (Fig. 1b). Significantly, this is very similar to the axis used for alkanethiol-based SAMs (i.e. SAMs that use long alkyl chains to determine orientation.) The 4 tetrahedral diamond lattice directions, with θ representing the polar and φ representing the azimuthal angle, can then be described as: **a**: θ=90°, φ=234.75°; **b**: θ=90°, φ=125.25°; **c**: 35.25°, φ=0°; **d**: 144.75°, φ=0°. These unit vectors are the approximate bond directions with respect to the molecular axis for the structures in the top row of figure 1. The bonds emanating from carbon centers, either parallel or antiparallel along these diamond lattice directions, are listed in table 1.

The second molecular axis selected in this study is coincident with the S-C bond of the diamondoid monomers, and lies along a diamond [111] lattice direction. Although the numbers of **a**, **b**, **c**, and **d** bonds remain unchanged upon selection of a different molecular axis, one must redefine the relative directions of these bonds and therefore the associated TDMs. When the molecular axis is defined along the S-C bond, for structure **1**, the bond directions become: **a**: θ=70.5°, φ=-90°; **b**: θ=180°, φ=0°; **c**: 70.5°, φ=150°; **d**: 70.5°, φ=30°. In structures **2-4**, with the molecular axis along the S-C bond, these directions become: **a**: θ=70.5°, φ=-120°; **b**: θ=70.5°, φ=120°; **c**: 70.5°, φ=0°; **d**: 180°, φ=0°. Each transition dipole moment, modeled along one of these diamond lattice directions, with respect to the *molecular* axis, in Cartesian coordinates, is denoted $\mathbf{M}_i$.

Ultimately, the desired goal is the molecular orientation, i.e. the tilt α, twist β, and sometimes also ϕ [1]. The relationship between the intensity of a NEXAFS resonance and the angles defining molecular orientation can be written in terms of the angle of incidence as follows:

Equation 4

$$I(\theta,\alpha,\beta,\phi)=$$

$$K\cdot\left[\sum_i\left(\begin{bmatrix}\sqrt{P}\cdot\sin(\theta)\\ \sqrt{1-P}\\ \sqrt{P}\cdot\cos(\theta)\end{bmatrix}^{\mathbf{T}}\begin{bmatrix}\cos(\phi) & -\sin(\phi) & 0\\ \sin(\phi) & \cos(\phi) & 0\\ 0 & 0 & 1\end{bmatrix}\begin{bmatrix}\cos(\alpha) & 0 & \sin(\alpha)\\ 0 & 1 & 0\\ -\sin(\alpha) & 0 & \cos(\alpha)\end{bmatrix}\begin{bmatrix}\cos(\beta) & -\sin(\beta) & 0\\ \sin(\beta) & \cos(\beta) & 0\\ 0 & 0 & 1\end{bmatrix}\cdot\mathbf{M}_i\right)^2\right]$$

where the respective rotation matrices are used on the dipole moments with respect to the molecular axis. Significantly, Equation 4 can be used or generalized to describe any molecule or set of molecules, and therefore, the equation is generally applicable to any SAM system. For the vast majority of SAMs studied with conventional NEXAFS, the azimuthal dependence can be averaged, since the domains are much smaller than the x-ray beam spot on the surface, and many surfaces, including Ag(111), nominally have three-fold symmetry, reducing Equation 4 to:

Equation 5

$$I(\Theta,\alpha,\beta) = K\left[\sum_i \left[(1-P\Theta)\left((\mathbf{G}_i\cdot\hat{x})^2+(\mathbf{G}_i\cdot\hat{y})^2\right)+2P\Theta(\mathbf{G}_i\cdot\hat{z})^2\right]\right]$$

where $\Theta=\cos^2(\theta)$ and

Equation 6

$$\mathbf{G}_i = \begin{bmatrix}\cos(\alpha) & 0 & \sin(\alpha)\\ 0 & 1 & 0\\ -\sin(\alpha) & 0 & \cos(\alpha)\end{bmatrix}\begin{bmatrix}\cos(\beta) & -\sin(\beta) & 0\\ \sin(\beta) & \cos(\beta) & 0\\ 0 & 0 & 1\end{bmatrix}\cdot\mathbf{M}_i$$

Note that Equation 5 deconvolutes the resonances into an in-surface-plane component, and a surface-normal component, and each term in the sum reduces to the "vector case" presented as equation 9.16 in ref. [1]. Equation 6 simply transforms all of the transition dipole moments with respect to the molecular axis into TDM's in the surface coordinate system, represented by $\mathbf{G}_i$.

Comparison of the relative experimental resonance intensity as a function of angle to the calculated NEXAFS angular dependence (Equations 5 and 6) is the core of the approach presented here. The experimental polarization-dependent resonances are deconvoluted from polarization independent features using a Monte Carlo approach to simultaneously fit the NEXAFS and the difference spectra[45]. By taking the ratios for the intensity of a single resonance at each angle of incidence to the intensity at a specific angle Θ_r (Equation 7), one can normalize for the transition and detection cross-sections (factor *K* in equations 3, 4 and 5), thereby eliminating the need to determine these values explicitly[1].

Equation 7

$$F(\Theta) = \frac{I(\Theta)}{I(\Theta_r)}$$

The function $F(\Theta)$, using a fixed Θ_r, is a linear function of Θ (see equation 5). Linear regressions of the experimental data reduced to the form of equation 7 yield the slope of this line, along with 95% high and low confidence limits[46]. One can also calculate the slope, or derivative, of $F(\Theta)$ for all combinations of molecular tilt and twist using Equations 5 and 6. Hence, comparison between the experimental and theoretical slopes for $F(\Theta)$, indicates the manifold of molecular tilt and twist combinations that are consistent with the NEXAFS data. For the purposes of this manuscript, any calculated slopes that fall within the 95% confidence limits of the experimental data represent possible diamondoid orientations.

Several assumptions are incorporated into the analysis. First, the intensity variation as a function of incident angle arises from a large ensemble of molecules, the majority of which are assumed to adopt a similar configuration on the surface. Contrary to this assumption, many SAMs

adopt a herringbone packing, i.e. two constituent molecular orientations with differing twist angles, or other similar multi-molecular unit cell arrangements[47-49]. Structural inhomogeneity can bias the NEXAFS-derived result towards a magic angle[1], or in this framework, a manifold of α and β where no polarization dependence would be observed. For diamondoids, with multi-directional TDMs and at the observed monolayer purities, this effect is minimal. The location of this manifold is useful to a qualitative analysis of the angular dependent resonances, and Figure 2 presents an example of these combinations of tilt and twist for tetramantane-6-thiol (structure **2**). Positive values of the slope of $F(\Theta)$ for C-H σ^* / R* resonances lie above and below these lines, while negative values lead to lines between these two lines, while the converse is true for the C-C σ^*. Inspection of the NEXAFS can thus instantly ascertain whether viable orientations lie above and below these two lines (e.g., for **2**, C-H σ^* most intense at normal incidence, C-C σ^* most intense at grazing incidence) or between these two lines (e.g., for **1**, C-H σ^* most intense at grazing incidence, C-C σ^* most intense at normal incidence).

A consideration of steric constraints is also essential to determine the physically viable subset of the orientations obtained from linear regression analysis of the experimental NEXAFS. The acquired S 2p core-level photoemission indicates that the diamondoid thiols are chemisorbed to the surface[6, 7, 39]. The sterically possible orientations are then found by simply modeling the molecule as anchored to the surface through the sulfur atom; all other atoms in the molecule must reside above the surface plane. In contrast, any calculated diamondoid atomic position lying below the surface plane for a particular molecular tilt/twist constitutes a sterically impossible orientation. The intersection of sterically feasible and NEXAFS-derived orientations gives all possible combinations of tilt and twist for the surface-attached molecules.

NEXAFS spectra from single, non-interacting thiol molecules were also simulated using the StoBe code[50]. The DFT code was applied with the generalized gradient approximation of Perdew-Burke-Ernzerhof (PBE) for the exchange/correlation functional[51]. The absorption was calculated for each carbon atom in a given molecule; this atom of interest was described by the IGLO-III basis[52] while the remainder of the carbons were modeled with effective core potentials[53] for the 1s electrons. For each atom, first, the equilibrium geometries were found in the ground state. Second, transition state (TS/TP) calculations were performed with 0.5 electronic charge in the core[54]. This calculation is used to determine the excitation spectrum. Finally, to calibrate energy scales between absorption from different carbon atoms within a molecule, the energy of the molecule with a core hole and an electron in the LUMO of the ground state was calculated for each carbon atom, and each atomic NEXAFS spectrum was shifted in energy such that the position of the first resonance is the total SCF energy difference between the calculated ground state and final state[43, 55]. Each angular dependent spectra was generated using the StoBe xrayspec utility by summing simulated spectra generated with three x-ray polarizations. These three polarizations, in the surface coordinate system, had polar angle equal to the incidence angle, and were at 120-degree intervals azimuthally. The discrete calculated resonances were convoluted with Gaussians of width 0.5 eV, below the ionization potential, and linearly increasing Gaussian width above the ionization potential to a maximum of 8 eV at 310 eV. The generated spectra were then shifted to higher energy to more closely match experiment by 1 eV, a value which is consistent with the average error between computation using PBE exchange/correlation functionals and experiment observed previously[56].

Results

Figure 3 displays the NEXAFS data for the series of thiolated diamondoids on silver surfaces. NEXAFS spectra were acquired at 20°(solid, red) 30° (dashed, orange) 40° (dashed, green) 55° (dashed, cyan) 70° (dashed, blue) and 90° (solid, purple). The differences between the acquired spectra and the spectrum at 20° are plotted just below the acquired spectra in order to accentuate the angular-dependent resonances. The observed angular-dependencies are small yet highly reproducible[6, 7, 39]. In all diamondoids, the C-H σ* / R* resonances are observed at about 287 – 289 eV while the broad set of C-C σ* has the most angular dependence in resonances centered at about 293 eV. These two manifolds of resonances are used to determine the molecular orientation. This series of diamondoids also exhibits the emergence of the bulk-diamond second gap band structure, characteristic of the diamondoids, at about 303 eV[13].

The top two series of angular dependent NEXAFS, both from [121] tetramantane derivatives, structures **1** and **2**, demonstrate control of diamondoid orientation through thiol substitution position. The observed angular dependencies arise because [121] tetramantanes contain a prevalence of C-C bonds generally aligned with the [110] long axis and a prevalence of C-H bonds in a plane orthogonal to this long axis. Structure **1**, with the thiol at the [2]-position on the side of the molecule, exhibits the greatest C-H σ* resonance intensity at close to grazing incidence (20°), while the C-C σ* is most intense at normal incidence (90°). Thus, this type of angular dependence qualitatively indicates a molecule that adopts a prostrate orientation on the Ag surface. In contrast, structure **2**, with the thiol at the end of the rod-like molecule, has the most intense C-H σ* / R* resonance at normal incidence, while the C-C σ* peak has the greatest intensity at grazing incidence. This is expected for an "upright" molecule (meaning the TDMs on average have a smaller polar angle than the magic angle[1], or in this case, magic manifold of angles) on the surface. Comparable angular-dependent behavior is observed for alkane thiol SAMs on gold, and both of these qualitative assignments of orientation are consistent with DFT-computed angular dependence resonances that will be discussed further in a subsequent section of this work.

The lower two series of angular dependent NEXAFS demonstrate how diamondoid structure affects angular dependence. Both diamondoids are pentamantanes. Structure **3**, derived from [1212]pentamantane, is similar to **1** and **2** with a prevalence of C-C bonds along, and C-H bonds orthogonal to the [110] direction. Structure **4**, however, is derived from [1(2,3)4]pentamantane, a molecule with T_d symmetry. Structure **3** exhibits strong angular dependence, and the NEXAFS is consistent with an upright molecular orientation, while little or no angular dependence is seen in the NEXAFS from structure **4**. This directly demonstrates diminishing NEXAFS angular dependence with increasing three-dimensional molecular symmetry; strong angular dependent resonances require a predominance of transition dipole moments along particular directions or in particular planes.

A more quantitative estimate of orientation on the surface can be derived for diamondoidthiolates on silver. The left panes of Figure 4 present the normalized intensity of the C-H σ* / R* (red) and C-C σ* (blue) resonances as a function of the cosine squared of the incidence angle. These data points are divided by the intensity of the same resonance acquired at 20° (see Equation 7). The linear regression is presented for each case, along with lines representing the 95% confidence limits for the slope of the regression. This experimental parameter, the slope of normalized intensity vs. $\cos^2(\theta)$, can also be simulated for a diamondoid of a given tilt and twist using the "building-block" approximation described above using Equations 5-7.

The 95% confidence limits define boundaries of the red and blue areas, which represent possible tilt/twist combinations, obtained for the C-H σ* / R* and C-C σ* resonances, respectively, in

the middle and right columns of Figure 4. These plots are generated in the following manner: A point by point simulation of the NEXAFS angular dependence for these two resonances is carried out using Equations 5-7, with $\Theta_r = \cos^2(20°)$. The slope of $F(\Theta)$ (Equation 7) at each tilt and twist is calculated, and compared to the experimental 95% confidence limits for this slope. Whenever a particular tilt/twist gives a slope within these limits, it is considered a viable orientation according to the NEXAFS. These bands thus implicitly incorporate an estimate of the error, in particular the precision of the measurement. Note the very narrow bands in structure 3, and the correspondingly precise linear fit, while structure 2 has both wider bands, and a less certain linear fit on the resonances. Along with the linear regression confidence limits, the molecular structure also influences precision. As an example, structure **4** has only the S-C bond breaking the T_d symmetry of [1(2,3)4]pentamantane-7-thiol, and minuscule angular dependences in the C-H σ* / R* and C-C σ* regions lead to very broad swaths of NEXAFS-determined tilt and twist.

By combining these viable tilt-twist bands with a geometric model of the sterically possible configurations, the actual orientations of the diamondoids can be estimated. The gray regions of the panes in the middle and right columns of Figure 4 represent these sterically acceptable combinations. The intensity of the red and blue bands increases when they intersect with sterically possible orientations to denote that these are the viable combinations of tilt and twist.

The middle and right columns of Figure 4 represent the estimated orientations of the diamondoid thiolates on silver using molecular axes along the long-axis [110] diamond crystallographic direction, and along the S-C bond, respectively. These panes have illustrations representative of feasible diamondoid orientations with the tilt and twist indicated. Note that the illustrated diamondoid orientations from the middle and right pane of a given specimen are identical; the only distinction is the molecular axis selected during analysis.

These diamondoids exhibit interesting structural differences, and provide a clear demonstration of the capabilities and limitations of NEXAFS to determine molecular orientation. In the top panes of figure 4, [121]tetramantane-2-thiol, structure **1**, exhibits a prostrate orientation, with an upright S-C bond. [121]tetramantane-6-thiol (**2**) is in an upright orientation with an S-C bond about 30 degrees from normal; a wide range of twist (β) is possible. These two [121]tetramantanes demonstrate the choice of thiol substitution position provides the ability to control orientation. The [1212]pentamantane-13-thiol (**3**) assumes an upright orientation. Overall, the [110] long axis is more normal to the surface than **2**, with a narrower range of possible polar angles, from about 50° at β = 0° to about 30° as β approaches a steric limit. The S-C bond is also only ~15° for $\beta < 60°$, indicating that the S-C bond is also more upright than **2**, however, the band also sweeps through the steric limit of ~45° as β increases. In the bottom column of Figure 4, the symmetric [1(2,3)4]pentamantane-7-thiol shows essentially no angular dependent changes, and the range of $F(\Theta)$ slopes is consistent with any orientation as determined through the C-C σ* spectral feature, and with this particular dataset, the C-H σ* / R* resonance leads to a very wide band of tilts and twists that does not overlap with the sterically accessible orientation. The orientation of this particular molecule cannot currently be determined with NEXAFS.

Discussion

The NEXAFS data gives insight into the possible orientations of tetramantane thiols and pentamantane thiols adsorbed on Ag. The diamondoids exhibit upright or prostrate orientation that is dependent upon the thiol substitution position and diamondoid isomer. Using a quantitative model,

under the assumption that most molecules in a particular monolayer assume similar configurations on the surface, diamondoids with a thiol moiety at the end or apical position (**2**, **3**) assume a generally upright orientation. Structure **2** has a very similar configuration on Ag as on Au[6], which is surprising given the strong influence the substrate typically has on monolayer structure. The three dimensional structure of the diamondoid and associated sterically restricted sulfur environment disallows the preferred sulfur configuration on Au[6], and thus on both Au and Ag substrates, the structure of the diamondoid itself, rather than sulfur-substrate bond, strongly influences the orientation. Also, NEXAFS cannot uniquely determine the twist on either substrate, and thus cannot prove that this parameter is the same on both Au and Ag. We have previously determined the S-C bond in **2** on Au to be about 30 +/- 10°[6, 7], and see similar results on Ag. Recent theory, however, predicts a less canted S-C bond than experiment for **2** on both Au and Ag[25]. Additional affects that were not explicitly computed, such as molecule-molecule interactions, various twist angles describing plausible orientation, and the hotly-debated true sulfur-metal configuration[57, 58] may affect the computed lowest-energy state of **2** on the surface, and may explain the discrepancy.

There are interesting differences between **2** and **3**: **3** has generally lower polar angles than **2** when considering both the [110] and S-C molecular axes. Note that the terminal cages in these two molecules are different. In **3**, the topmost cage adds lateral bulk, especially in the general tilt and twist ($-90° < \beta < 90°$) directions that are indicated as plausible by the NEXAFS. This can be seen in the leftmost illustrations of **2** and **3** in Figure 4: in contrast to **2**, the topmost adamantane cage in **3** protrudes to the right. We speculate that the packing on the surface of the bulkier **3** compared to **2** causes the upright orientation observed for **3**.

Although **1** could assume a more canted S-C bond similar to apical cases (cf. Fig. 4, top right pane, twist angle of ~ 270°) the NEXAFS does not overlap this sterically accessible region. In the twist angles where NEXAFS does overlap (60 – 210°), the diamondoid resides in a more sterically restricted environment, with maximum possible tilt of about 15°. The configuration is also very similar to what was derived previously, and as on gold, structure **1** may have a complex or even incommensurate relationship to the underlying lattice. Once chemisorbed on the surface this molecule exhibits two enantiomers, which could presumably lead to a lack of order, i.e., an irregular surface-pattern. This does not eliminate the potential for orientational similarity.

Computed x-ray absorption spectra support the results of the tilt-twist analysis. Figure 5 presents computed near-edge x-ray absorption angular dependent spectra for the series of diamondoid thiols **1**-**4** (Figure 1). For each molecule, simulated NEXAFS traces at 20, 30, 40 55, 70 and 90º incidence angle are shown. The lower difference spectra traces have the 20º trace subtracted to emphasize the angular dependence. The computed spectra are calculated for the specific tilt (α) and twist (β) indicated. These were chosen based on the results presented in Figure 4 and refined according to spectral similarity with the experimental data presented in Figure 3. Overall, the computed x-ray absorption spectra match experiment. Particularly striking are the polarization-dependent resonances as seen in the difference spectra. For molecule **1**, two resolvable features appear in the C-H σ^* / R* region of the difference spectra and are more intense at grazing incidence, matching experiment remarkably well. The C-C σ^* exhibits angular dependence on the high-energy side of the resonance both in computed and experimental data, and this region is generally more intense at normal than at grazing incidence. For molecule **2**, the opposite angular dependence is observed in the theoretical spectra as expected for an upright, rather than prostrate diamondoid, and the resonances are spread more uniformly over the C-H σ^* / R* and especially the C-C σ^* area in both **2** and **3**. A peak that is highly convoluted with the manifold of C-H σ^* / R*, very near and/or at the absorption onset, has opposite angular dependence as seen by the small dip in the experimental data; this is reproduced

in the computed spectra. Finally, in **4** the computed spectra exhibit very little polarization dependence as expected, but the very small variations with angle appear to reproduce the experimental data. Thus, the derived orientations are consistent with simulated NEXAFS of molecules in these particular orientations.

For all of the diamondoid thiols, additional complementary results, such as STM, will be valuable in determining the structure of diamondoid thiol self-assembled monolayers. One of the major assumptions made in interpreting the NEXAFS is that each diamondoid in a monolayer adsorbs in similar orientational conformation, and this is not evident from these results alone. The strength of this framework is that it is quantitative, and even for a multi-phase (e.g. surface dimer) SAM, the technique gives a NEXAFS-weighted average orientation of the molecules on the surface. Further, the framework can be extended to include multiple diamondoid orientations.

The precision of this framework is determined by the quality of the data and the molecular structure analyzed. This is clearly observed for **4** where the high symmetry of the molecule adversely affects the attainable precision. Any tilt-twist combination lies within the 95% confidence limits of the angular dependence of the C-C σ*, while the wide band of the C-H σ* / R* does not overlap the sterically possible combinations of the molecular tilt and twist. This is the extreme case, however, as essentially no other SAMs studied to date have been composed of molecules with such a high level of symmetry within the individual molecular structures. One potential pathway to resolve the structure of this SAM would be to selectively functionalize the diamondoid on the face opposing the thiol with, for example, carboxyl, alcohol, or another functional group, and then use the additional resonances from other x-ray absorption edges to resolve the tilt and twist. The NEXAFS from other diamondoid thiols in this work also exhibit less angular dependence than typical SAMs, but produce reasonable precision in tilt/twist angles. In structures **1**-**3**, these bands are typically around 10-20° in width, but sometimes produce precision as small as a few degrees, especially in the C-H σ* / R* resonance. The accuracy of the method, however, is not as good as the precision, and error in accuracy is estimated to be an additional +/- 5° in structures **1**-**3**. First, systematic errors in acquiring and reducing the experimental data lead to some variation of the derived tilts and twists[39]. Second, the assumptions and approximations in determining and interpreting transition dipole moments must also be considered in estimating the accuracy of the results. Characterization of these phenomena in diamondoid thiols and other complex molecules adsorbed on surfaces provides understanding that is of fundamental importance in the development and optimization of robust monolayers for technological applications. The presented framework will be useful in determining the orientation of essentially any rigid and oriented molecular structures on surfaces.

Conclusions

A framework for using NEXAFS to determine two parameter orientations (in this case, tilt and twist) from rigid molecules with arbitrary shape has been used on diamondoid thiolates adsorbed on silver. The framework reveals orientationally ordered diamondoid SAMs with high precision, despite the weak NEXAFS angular dependence in diamondoids. The molecular orientation is controlled by the thiol substitution position and diamondoid shape. Through the analysis of NEXAFS spectra, [121]tetramantane-2-thiol on Ag, with the thiol positioned at the side, has a prostrate orientation, where the sulfur-carbon bond is approximately normal to the surface, with a polar angle of less than 15°. In contrast, higher diamondoids with thiols at the end, or apical positions, namely [121]tetramantane-6-thiol and [1212]pentamantane-13-thiol, are upright on the Ag surface, with sulfur-

carbon polar angles of about 30° +/- 15° for the tetramantane and about 15° +/- 10° (with 0° twist) for the pentamantane. Finally, the limitations of the framework and NEXAFS in general are demonstrated by the inability in both precision, and in accuracy, to determine orientation of the highly symmetric [1(2,3)4]pentamantane-7-thiol on Ag. This work demonstrates control over the assembly, in particular the orientational and electronic structure, and therefore the surface properties of this exciting new class of nanodiamond materials.

Acknowledgements

We thank the staff of SSRL especially Dan Brehmer and Curtis Troxel. We acknowledge assistance and advice in computing XAS spectra from the StoBe authors Klaus Hermann and Lars Pettersson. This work was funded by the Office of Basic Energy Sciences, Materials Sciences, U. S. Department of Energy. Research was performed at the Stanford Synchrotron Radiation Laboratory, a national user facility operated by Stanford University on behalf of the U.S. D.O.E., Office of Basic Energy Sciences. This work was partially performed under the auspices of the U.S. Department of Energy by Lawrence Livermore National Laboratory under Contract DE-AC52-07NA27344. Work performed at the Justus-Liebig University was supported by the Fonds der Chemischen Industrie and the Deutsche Forschungsgemeinschaft.

References

[1] J. Stöhr, NEXAFS Spectroscopy, Springer-Verlag, Berlin - Heidelberg - New York, 1992.
[2] N. Ballav, B. Schüpbach, O. Dethloff, P. Feulner, A. Terfort and M. Zharnikov, JACS 129 (2007) 15416-15417.
[3] Y. Zou, T. Araki, G. Appel, A.L.D. Kilcoyne and H. Ade, Chem. Phys. Lett. 430 (2006) 287-292.
[4] J.X. Fu and S.G. Urquhart, J. Phys. Chem. A 109 (2005) 11724-11732.
[5] G. Hähner, M. Kinzler, C. Wöll, M. Grunze, M. K. Scheller and L.S. Cederbaum, Phys. Rev. Lett. 67 (1991) 851.
[6] T.M. Willey, J.D. Fabbri, J.R.I. Lee, P.R. Schreiner, A.A. Fokin, B.A. Tkachenko, N.A. Fokina, J.E.P. Dahl, R.M.K. Carlson, A.L. Vance, W.L. Yang, L.J. Terminello, T. Van Buuren and N.A. Melosh, JACS 130 (2008) 10536-10544.
[7] W.L. Yang, J.D. Fabbri, T.M. Willey, J.R.I. Lee, J.E. Dahl, R.M.K. Carlson, P.R. Schreiner, A.A. Fokin, B.A. Tkachenko, N.A. Fokina, W. Meevasana, N. Manella, K. Tanaka, X.J. Zhou, T. Van Buuren, M.A. Kelly, Z. Hussain, N.A. Melosh and Z.X. Shen, Science 316 (2007) 1460-1462.
[8] J.R.I. Lee, T.Y.J. Han, T.M. Willey, D. Wang, R.W. Meulenberg, J. Nilsson, P.M. Dove, L.J. Terminello, T. Van Buuren and J.J. De Yoreo, JACS 129 (2007) 10370-10381.
[9] J.R.I. Lee, T.M. Willey, J. Nilsson, L.J. Terminello, J.J. De Yoreo and T. Van Buuren, Langmuir 22 (2006) 11134-11141.
[10] H. Schwertfeger, A.A. Fokin and P.R. Schreiner, Angew. Chem. Int. Ed. 47 (2008) 1022-1036.
[11] J.E. Dahl, S.G. Liu and R.M.K. Carlson, Science 299 (2003) 96-99.
[12] B.A. Tkachenko, N.A. Fokina, L.V. Chernish, J.E.P. Dahl, S.G. Liu, R.M.K. Carlson, A.A. Fokin and P.R. Schreiner, Org. Lett. 8 (2006) 1767-1770.
[13] T.M. Willey, C. Bostedt, T. Van Buuren, J.E. Dahl, S.G. Liu, R.M.K. Carlson, L.J. Terminello and T. Moller, Phys. Rev. Lett. 95 (2005) 113401.
[14] Y. Wang, E. Kioupakis, X. Lu, D. Wegner, R. Yamachika, J.E. Dahl, R.M.K. Carlson, S.G. Louie and M.F. Crommie, Nat. Mater. 7 (2008) 38-42.
[15] T.M. Willey, C. Bostedt, T. Van Buuren, J.E. Dahl, S.G. Liu, R.M.K. Carlson, R.W. Meulenberg, E.J. Nelson and L.J. Terminello, Phys. Rev. B 74 (2006) 205432.
[16] K. Klünder, Photoelectron Spectroscopy on Molecular Diamond, Diploma Thesis, Department of Physics, Technical University of Berlin, 2007.
[17] T. Van Buuren, L.N. Dinh, L.L. Chase, W.J. Siekhaus and L.J. Terminello, Phys. Rev. Lett. 80 (1998) 3803-3806.
[18] A.J. Williamson, C. Bostedt, T. Van Buuren, T.M. Willey, L.J. Terminello and G. Galli, Nano Lett. 4 (2004) 1041-1045.
[19] K. Lenzke, L. Landt, M. Hoener, H. Thomas, J.E. Dahl, S.G. Liu, R.M.K. Carlson, T. Moller and C. Bostedt, J. Chem. Phys. 127 (2007) 084320.
[20] G.C. Mcintosh, M. Yoon, S. Berber and D. Tomanek, Phys. Rev. B 70 (2004) 045401.
[21] N.D. Drummond, A.J. Williamson, R.J. Needs and G. Galli, Phys. Rev. Lett. 95 (2005) 096801.
[22] A.J. Lu, B.C. Pan and J.G. Han, Phys. Rev. B 72 (2005) 035447.
[23] A.A. Fokin and P.R. Schreiner, Mol. Phys. 107 (2009, in press)
[24] W.A. Clay, Z. Liu, W.L. Yang, J.D. Fabbri, J.E. Dahl, R.M.K. Carlson, Y. Sun, P.R. Schreiner, A.A. Fokin, B.A. Tkachenko, N.A. Fokina, P.A. Pianetta, N. Melosh and Z.X. Shen, Nano Lett. 9 (2009) 57-61.
[25] W.H. Zhang, B. Gao, J.L. Yang, Z.Y. Wu, V. Carravetta and Y. Luo, J. Chem. Phys. 130 (2009) 054705.

[26] J.C. Love, L.A. Estroff, J.K. Kriebel, R.G. Nuzzo and G.M. Whitesides, Chem. Rev. 105 (2005) 1103-1169.
[27] S. Fujii, U. Akiba and M. Fujihira, JACS 124 (2002) 13629-13635.
[28] A.A. Dameron, L.F. Charles and P.S. Weiss, JACS 127 (2005) 8697-8704.
[29] A.A. Dameron, T.J. Mullen, R.W. Hengstebeck, H.M. Saavedra and P.S. Weiss, J. Phys. Chem. C 111 (2007) 6747-6752.
[30] A.A. Dameron, J.R. Hampton, S.D. Gillmor, J.N. Hohman and P.S. Weiss, J. Vac. Sci. Technol., B 23 (2005) 2929-2932.
[31] A.A. Dameron, J.R. Hampton, R.K. Smith, T.J. Mullen, S.D. Gillmor and P.S. Weiss, Nano Lett. 5 (2005) 1834-1837.
[32] P.R. Schreiner, N.A. Fokina, B.A. Tkachenko, H. Hausmann, M. Serafin, J.E.P. Dahl, S.G. Liu, R.M.K. Carlson and A.A. Fokin, J. Org. Chem. 71 (2006) 6709-6720.
[33] A.A. Fokin, B.A. Tkachenko, P.A. Gunchenko, D.V. Gusev and P.R. Schreiner, Chem. Eur. J. 11 (2005) 7091-7101.
[34] A.A. Fokin, P.R. Schreiner, N.A. Fokina, B.A. Tkachenko, H. Hausmann, M. Serafin, J.E.P. Dahl, S.G. Liu and R.M.K. Carlson, J. Org. Chem. 71 (2006) 8532-8540.
[35] H. Schwertfeger, C. Würtele, M. Serafin, H. Hausmann, R.M.K. Carlson, J.E.P. Dahl and P.R. Schreiner, J. Org. Chem. 73 (2008) 7789-7792.
[36] T.M. Willey, A.L. Vance, T. Van Buuren, C. Bostedt, L.J. Terminello and C.S. Fadley, Surf. Sci. 576 (2005) 188-196.
[37] K.G. Tirsell and V.P. Karpenko, Nuclear Instruments & Methods in Physics Research Section a-Accelerators Spectrometers Detectors and Associated Equipment 291 (1990) 511-517.
[38] V. Karpenko, J.H. Kinney, S. Kulkarni, K. Neufeld, C. Poppe, K.G. Tirsell, J. Wong, J. Cerino, T. Troxel and J. Yang, Rev. Sci. Instrum. 60 (1989) 1451-1456.
[39] See Supporting Information, available at http://www.sciencedirect.com/).
[40] J. Stohr and D.A. Outka, Phys. Rev. B 36 (1987) 7891-7905.
[41] T. Schiros, L.Å. Näslund, K. Andersson, J. Gyllenpalm, G.S. Karlberg, M. Odelius, H. Ogasawara, L.G.M. Pettersson and A. Nilsson, J. Phys. Chem. C 111 (2007) 15003-15012.
[42] H. Öström, L. Triguero, M. Nyberg, H. Ogasawara, L.G.M. Pettersson and A. Nilsson, Phys. Rev. Lett. 91 (2003) 046102.
[43] C. Kolczewski, F.J. Williams, R.L. Cropley, O.P.H. Vaughan, A.J. Urquhart, M.S. Tikhov, R.M. Lambert and K. Hermann, J. Chem. Phys. 125 (2006) 034701.
[44] F.A. Asmuruf and N.A. Besley, J. Chem. Phys. 129 (2008) 064705.
[45] T.M. Willey, A.L. Vance, T. Van Buuren, C. Bostedt, A.J. Nelson, L.J. Terminello and C.S. Fadley, Langmuir 20 (2004) 2746-2752.
[46] J.R. Taylor, An Introduction to Error Analysis: The Study of Uncertainties in Physical Measurements, University Science Books, 1982.
[47] D. Kafer, G. Witte, P. Cyganik, A. Terfort and C. Wöll, JACS 128 (2006) 1723-1732.
[48] P. Cyganik, K. Szelagowska-Kunstman, A. Terfort and M. Zharnikov, J. Phys. Chem. C 112 (2008) 15466-15473.
[49] P. Jiang, A. Nion, A. Marchenko, L. Piot and D. Fichou, JACS 128 (2006) 12390-12391.
[50] K. Hermann, L.G.M. Pettersson, M.E. Casida, C. Dual, A. Goursot, A. Koester, E. Proynov, A. St-Amant, D.R. Salahub, V. Carravetta, H. Duarte, C. Friedrich, N. Godbout, J. Guan, C. Jamorski, M. Leboeuf, M. Leetmaa, M. Nyberg, S. Patchkovskii, L. Pedocchi, F. Sim, L. Triguero and A. Vela, StoBe-deMon version 3.0, 2007, http://www.rz-berlin.mpg.de/~hermann/StoBe/
[51] J.P. Perdew, K. Burke and M. Ernzerhof, Phys. Rev. Lett. 77 (1996) 3865-3868.

[52] W. Kutzelnigg, U. Fleischer and M. Schindler, The IGLO-Method: Ab Initio Calculation and Interpretation of NMR Chemical Shifts and Magnetic Susceptibilities, Springer-Verlag, Heidelberg, 1990.
[53] L.G.M. Pettersson, U. Wahlgren and O. Gropen, J. Chem. Phys. 86 (1987) 2176-2184.
[54] L. Triguero, L.G.M. Pettersson and H. Agren, Phys. Rev. B 58 (1998) 8097-8110.
[55] C. Kolczewski, R. Puttner, O. Plashkevych, H. Agren, V. Staemmler, M. Martins, G. Snell, A.S. Schlachter, M. Sant'anna, G. Kaindl and L.G.M. Pettersson, J. Chem. Phys. 115 (2001) 6426-6437.
[56] O. Takahashi and L.G.M. Pettersson, J. Chem. Phys. 121 (2004) 10339-10345.
[57] R. Mazzarello, A. Cossaro, A. Verdini, R. Rousseau, L. Casalis, M.F. Danisman, L. Floreano, S. Scandolo, A. Morgante and G. Scoles, Phys. Rev. Lett. 98 (2007) 016102.
[58] P. Maksymovych, D.C. Sorescu and J.T. Yates, Phys. Rev. Lett. 97 (2006) 146103.

Table 1: Table of bond directions, originating at C atomic centers, and aligned along indicated bond directions, used in this work. The C-S bond is tallied with the C-C bonds.

	C-H bonds				C-C/S bonds			
Structure	**a**	**b**	**c**	**d**	**a**	**b**	**c**	**d**
1	9	10	6	2	13	12	16	20
2	10	10	6	1	12	12	16	21
3	12	12	4	3	14	14	22	23
4	8	8	8	7	18	18	18	19

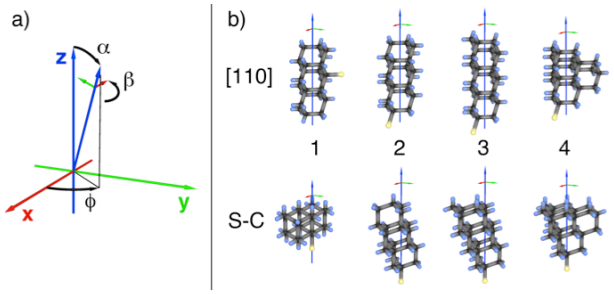

Figure 1. a) Definition of the molecular axis and the angles defining the molecular orientation: tilt or polar angle (a for tilt or polar angle polar angle (α), twist or dihedral angle (β), and azimuthal angle (φ). **b)** The thiolated higher diamondoids studied in this work: **1**: [121] tetramantane-2-thiol, **2**: [121]tetramantane-6-thiol, **3**: [1212]pentamantane-13-thiol, and **4**: [1(2,3)4]pentamantane-7-thiol. To define molecular orientation, an arbitrary molecular axis is chosen; in this case, two convenient axes are: along the long axis of **1**, **2**, and **3** that is parallel to one of the [110] diamond crystallographic directions (top) and along the sulfur-carbon bond, along one of the diamond [111] directions, denoted S-C in the lower figures.

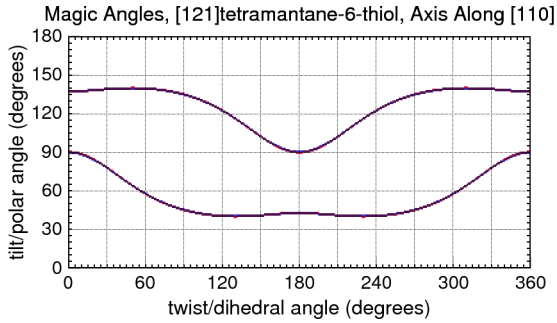

Figure 2: Manifold of tilts and twists that will lead to no angular dependence in NEXAFS resonances for structure **2**. (See Figure 1 b), [110] molecular axis.) These angles are analogous to the so-called "magic angle" which for a single vector-type resonance or a set of resonances in a plane, with high beam polarization, is about 54.7°[1].

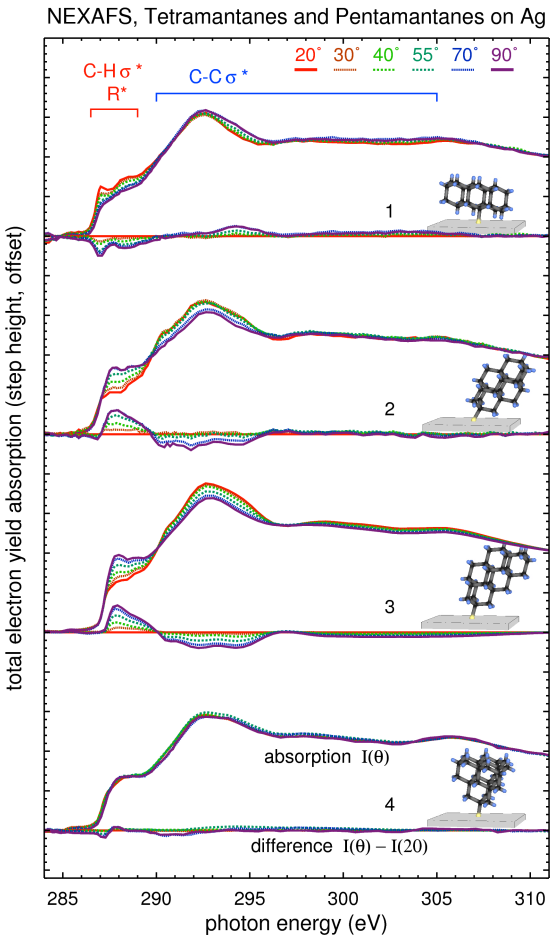

Figure 3: Near-edge x-ray absorption fine structure spectra for the series of diamondoid thiols **1**–**4** (Figure 1). For each molecule, the NEXAFS traces at 20, 30, 40 55, 70 and 90º incidence angle are shown. The lower traces have the 20º trace subtracted to emphasize the angular dependence.

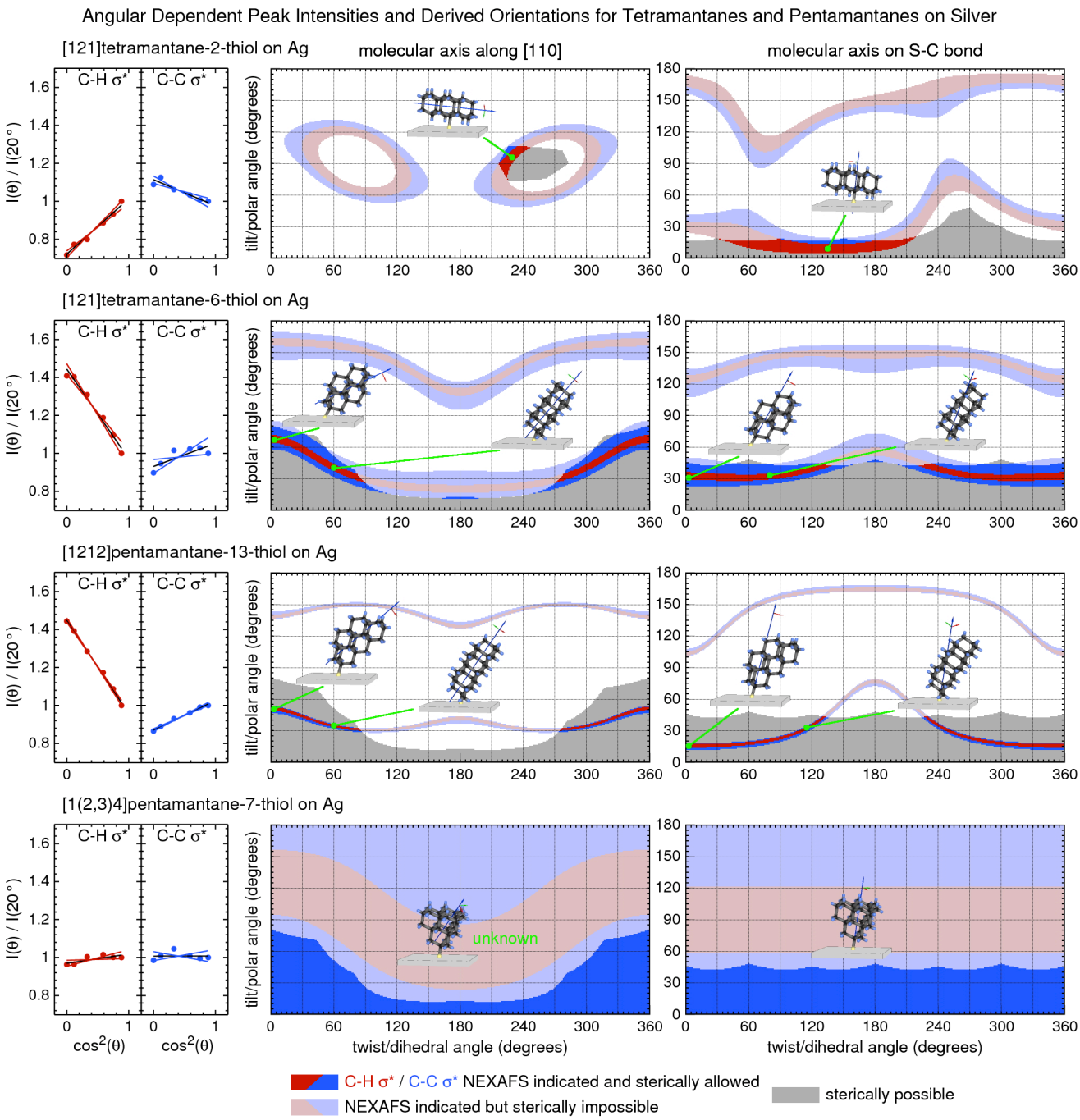

Figure 4: Left panes: the intensity of angular dependent C-H σ* / R* and C-C σ* resonances normalized to the resonance collected at 20°. These are plotted vs. the cosine squared of the incident angle θ. The linear regression (black) and 95% confidence limits of the slope of the linear regression (red and blue for C-H σ* and C-C σ* respectively) are also plotted. In the right panes, these confidence limit slopes are used to determine manifolds of plausible molecular tilt and twist. Red bands correspond to C-H σ*, blue to C-C σ*. These NEXAFS bands are compared to the sterically possible orientations of the diamondoid thiolate on the surface, denoted by gray areas. Different molecular axes are used to gain insight; in the middle panes, the axes are chosen along a diamond [110] direction, similar to alkanethiolate SAMs. On the right, the molecular axis is chosen along the S-C bond of the molecule. Pictoral representations of some of the orientations at different possible tilts and twists are also presented. Due to high symmetry, difficulty arises in determining the orientation of [1(2,3)4]pentamantane-7-thiolate.

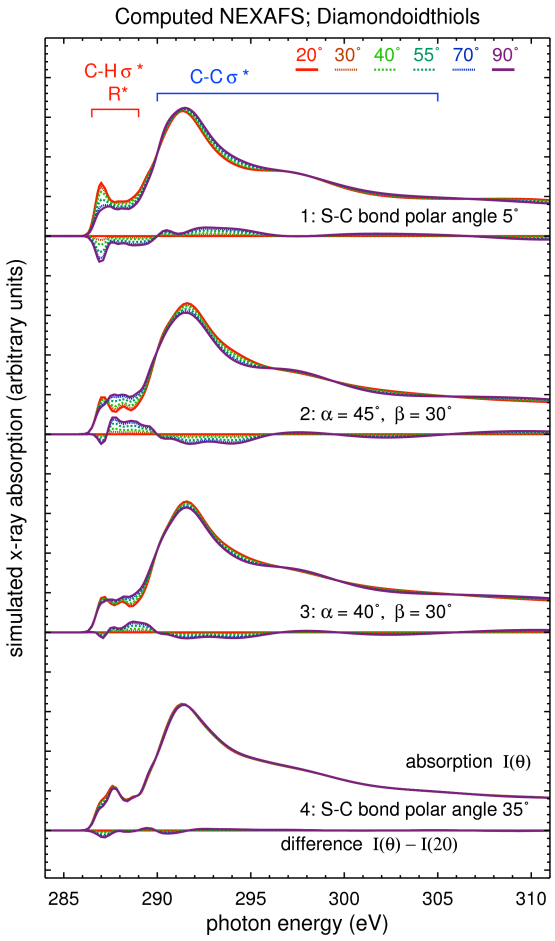

Figure 5: Computed near-edge x-ray absorption fine structure spectra for the series of diamondoid thiols **1**–**4** (Figure 1). For each molecule, the NEXAFS traces at 20, 30, 40 55, 70 and 90º incidence angle are shown. The lower difference spectra traces have the 20º trace subtracted to emphasize the angular dependence. The computed spectra are calculated for the specific tilt (α) and twist (β) indicated. These were chosen based on the results presented in Figure 4 and refined according to spectral similarity with the experimental data presented in Figure 3.

Supporting Information

Determining Orientational Structure of Diamondoid Thiols Attached to Silver Using Near-Edge X-ray Absorption Fine Structure Spectroscopy

Trevor M. Willey[1*], Jonathan R. I. Lee[1], Jason D. Fabbri[2],
Dongbo Wang[3], Michael H. Nielsen[4], Jason C. Randel[2],
Peter R. Schreiner[5], Andrey A. Fokin[5], Boryslav A. Tkachenko[5], Nataliya A. Fokina[5],
Jeremy E. P. Dahl[6], Robert M. K. Carlson[6],
Louis J. Terminello[1], Nicholas A. Melosh[2], and Tony van Buuren[1]

1) Materials and Condensed Matter Division, Lawrence Livermore National Laboratory, 7000 East Avenue, Livermore CA 94550
2) Stanford University, 476 Lomita Mall, Stanford, CA 94305
3) Department of Geosciences, Virginia Tech, Blacksburg, VA 24061
4) University of California, Davis, CA 95616
5) Institute of Organic Chemistry, Justus-Liebig University Giessen, Heinrich-Buff-Ring 58, 35392 Giessen, Germany
6) MolecularDiamond Technologies, Chevron Technology Ventures, 100 Chevron Way, Richmond, CA 94802

* e-mail address: willey1@llnl.gov

Plots Of Orientation that would Lead to No NEXAFS Angular Dependence

These plots indicate the "magic manifolds" or combinations of tilt and twist for the 4 diamondoids studied which would lead to no angular dependence. These were found by observing the intensity as a function of the cosine squared of the incident angle. More specifically, observing where the slope, found by

$$\frac{\frac{I(\theta)}{I(20°)} - 1}{\cos^2(\theta) - \cos^2(20°)}$$

is close to zero.

The plots also compare "building-block" and DFT-computed transition dipole moments. The black line represents the calculation by considering TDM's to lie along sigma bonds in the molecule (building block). The red and blue are preliminary results by using computed spectra generated by the StoBe DFT code as outlined in the text. The red are the result of integrating over the intensities in the C-H σ* / R* region, while the blue integrate over the C-C σ* region. Due to the more involved calculation, these were computed at 4 degree intervals in tilt and twist. For samples 1, 2, and 3, an absolute value of slope from the above equation with a value less than (arbitrarly chosen) 0.02 or 0.01 (for the C-H σ* / R* and C-C σ* regions, respectively) are plotted. The constants were reduced in the case of sample 4, but the slopes are still smaller at any orientation in the C-C σ* region.

These preliminary results also indicate that for the diamondoids in this particular case, the building block approximation is sufficient to give an estimate molecular orientation.

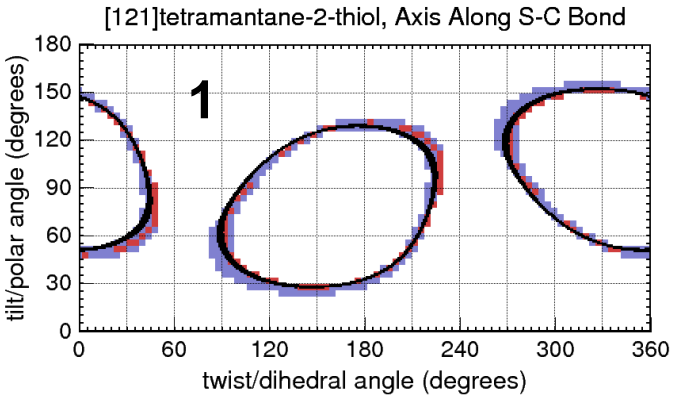

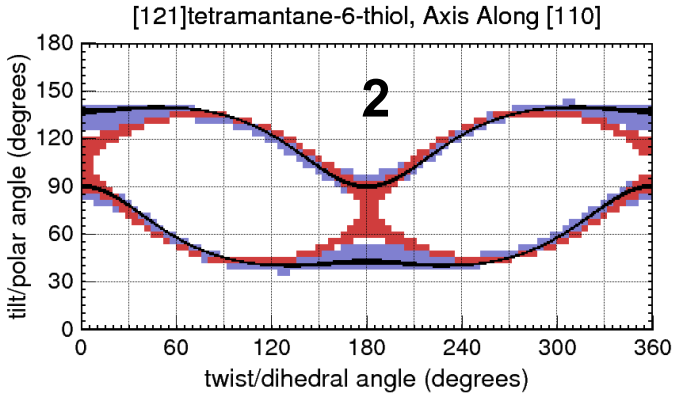

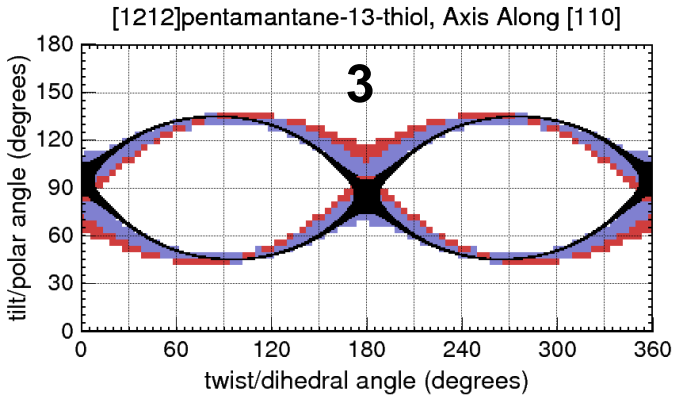

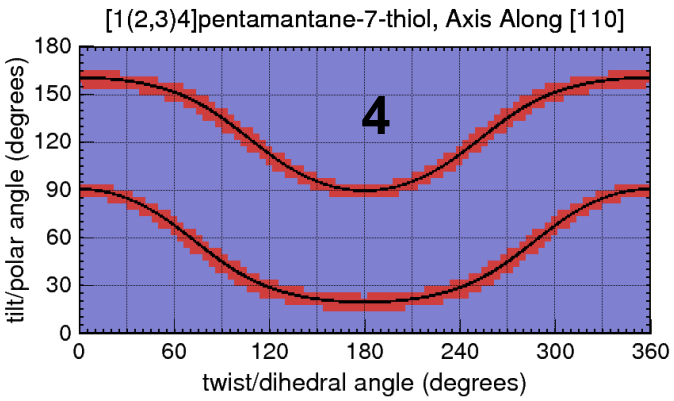

Plots Of Contour Lines, Positive and Negative Slopes of $I(\theta)/I(20^{o})$ vs $\cos^2(\theta)$

This is a plot of contour lines of specific slopes for the C-H (red) and C-C σ* (blue) resonances for [121]tetramantane-6-thiol, as a function of the cosine squared of incident angle, all divided by the resonance at 20 degrees, as presented in the text. This figure augments figure 2 in the text. The tilts and twists that would give no polarization dependence are plotted as purple lines, as in Figure 2. Additionally, positive slopes for the C-H are between the lines, while negative lie above and below. The converse is true for the C-C resonance.

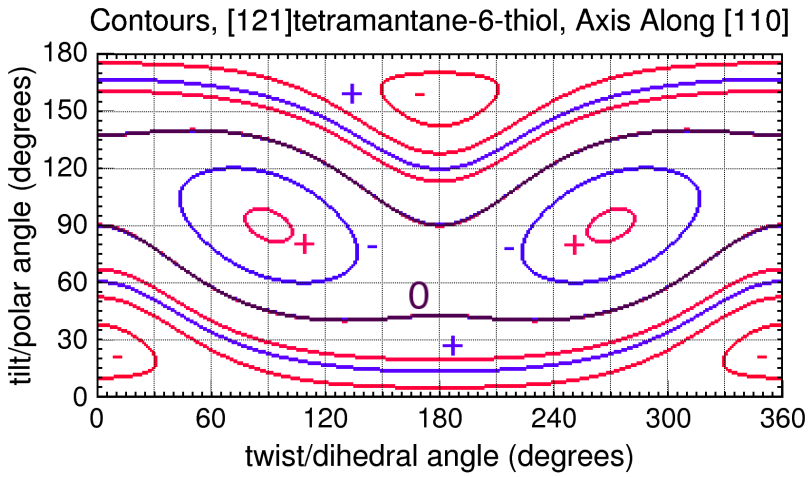

Additional NEXAFS Data

Presented are the data for [121]tetramantane-2-thiol on Ag (top two panes) and on Au (lower two panes). Below are the resonant intensities as well as the derived orientations, in similar fashion as figure 4.

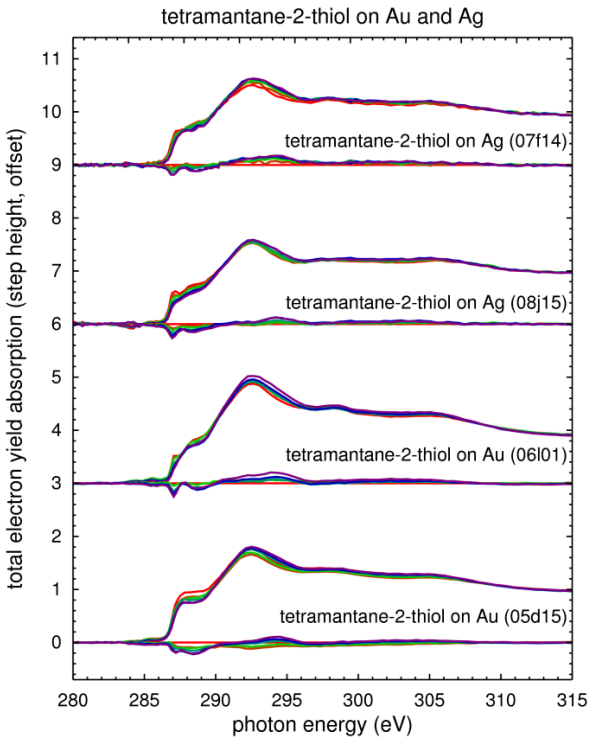

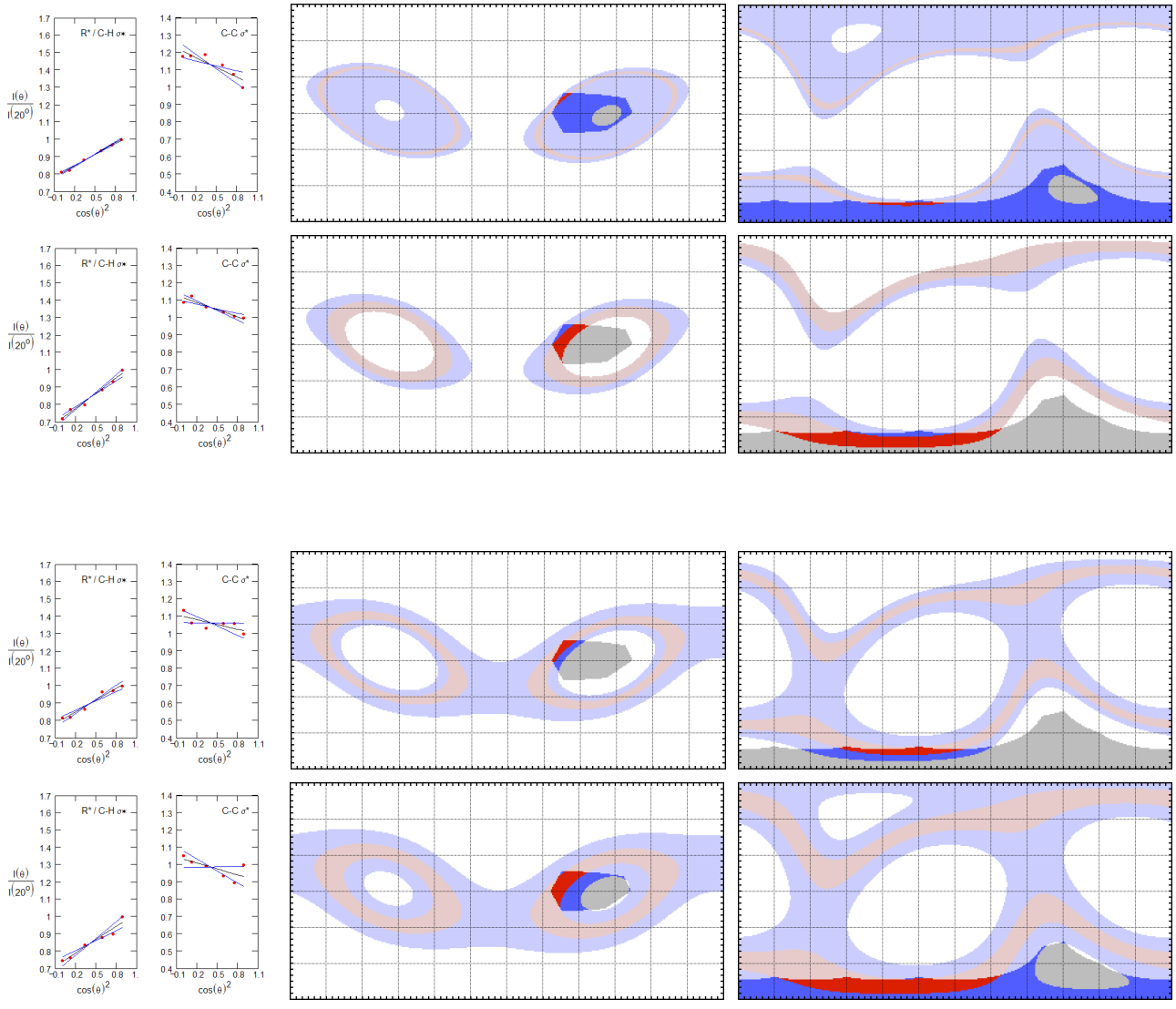

Additional NEXAFS Data

Presented are the data for [121]tetramantane-6-thiol on Ag (top two panes) and on Au (lower two panes). Below are the resonant intensities as well as the derived orientations, in similar fashion as figure 4.

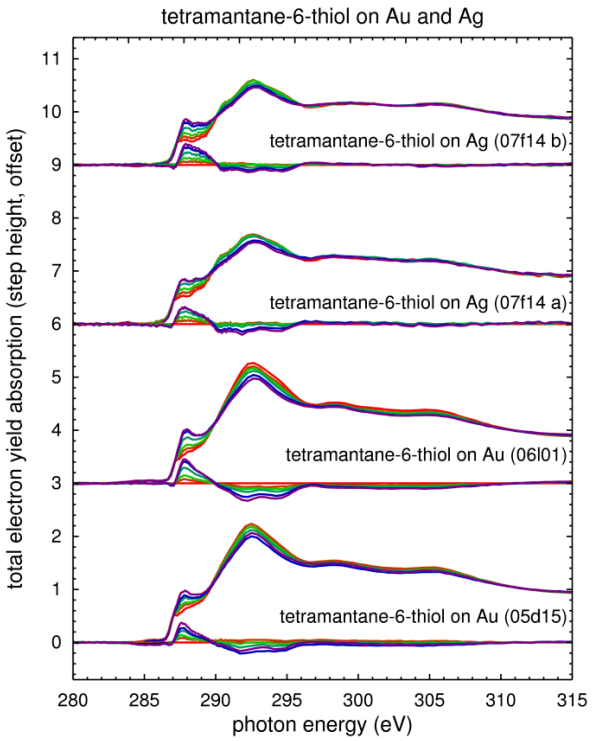

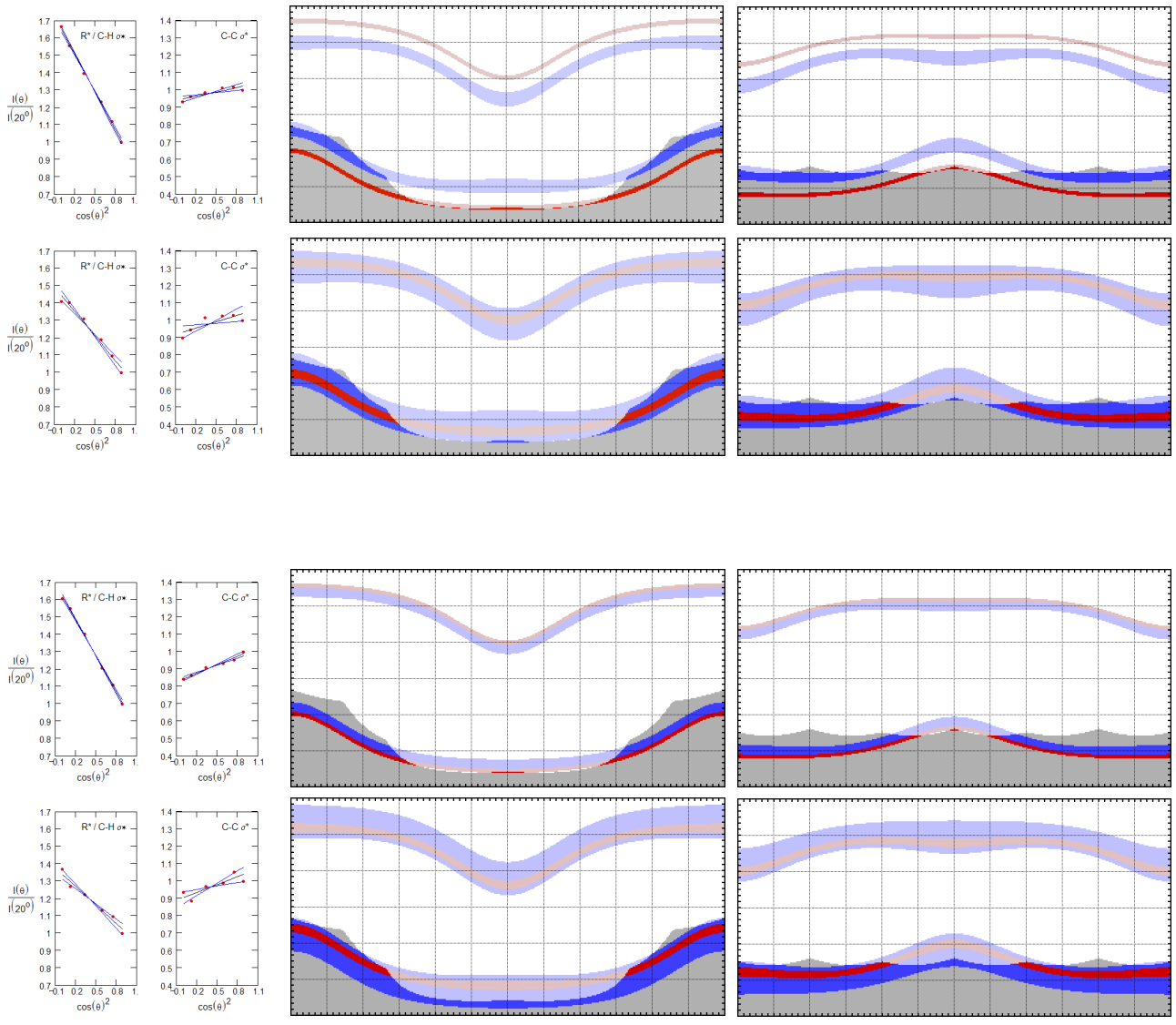

Additional NEXAFS Data

Presented are the data for [1212]pentamantane-13-thiol on Ag (top two panes) and on Au (lower two panes). Below are the resonant intensities as well as the derived orientations, in similar fashion as figure 4.

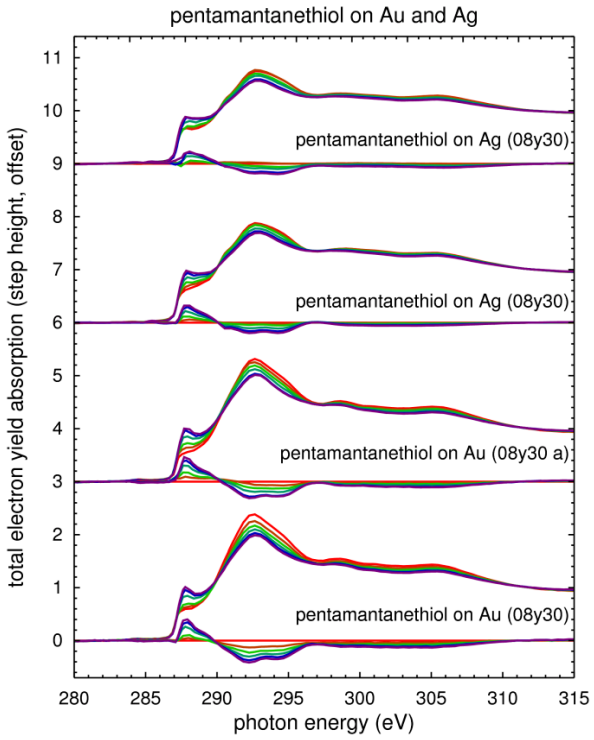

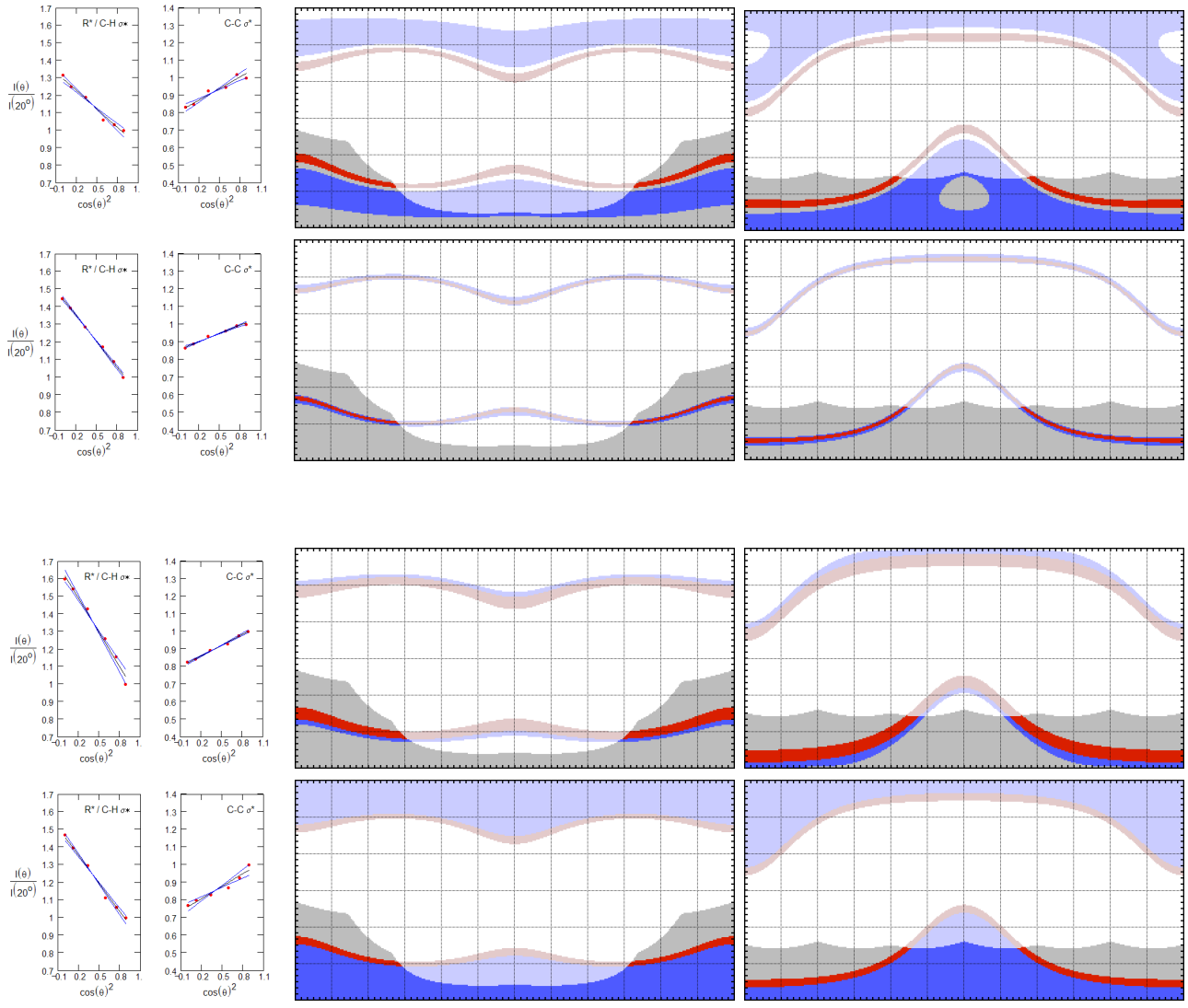

Additional NEXAFS Data

Presented are the data for [1(2,3)4]pentamantane-7-thiol on Ag (top two panes) and on Au (lower two panes). The top Ag trace is believed to have significant contamination in the monolayer and/or the normalization clean Ag surface. The two lower scans on Au also may have had some slight contamination. Below are the resonant intensities. The derived orientations are meaningless as they either cover any sterically possible orientation (top, Ag and bottom Au) or overlap with no possible orientations as in the rest of the resonances. The plots consider a molecular axis along the S-C bond, in similar fashion as figure 4.

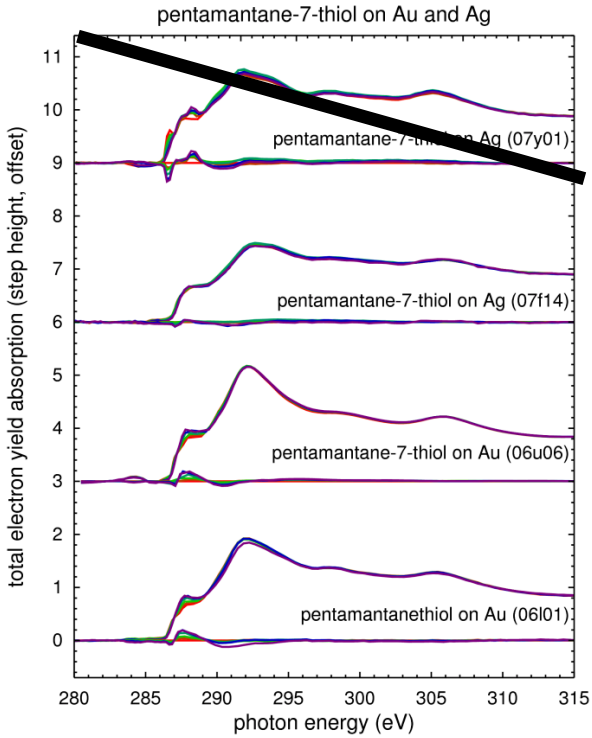

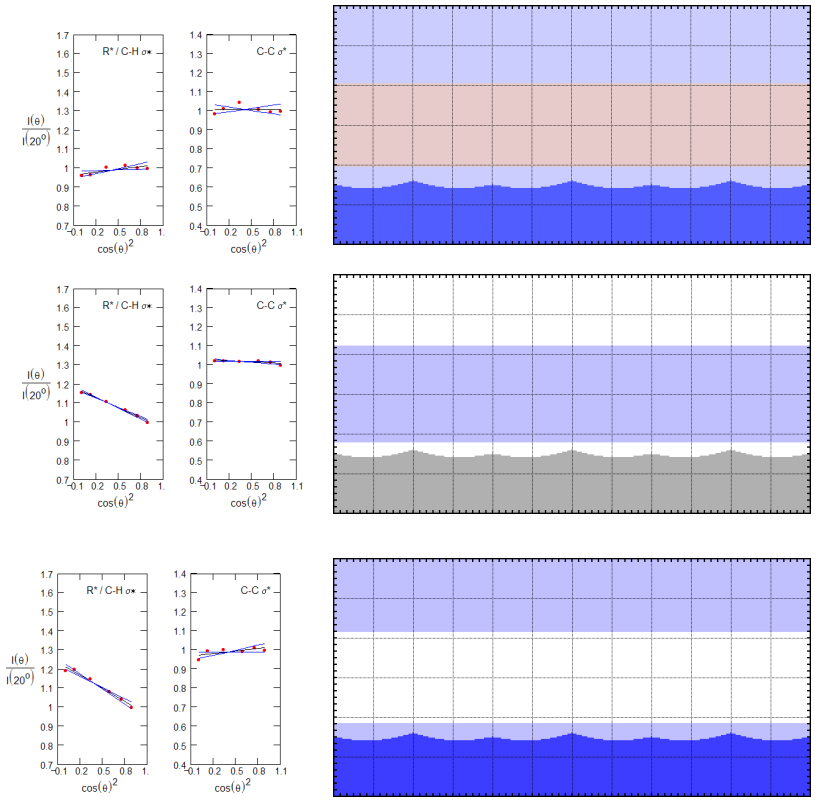

Sulfur 2p XPS data

Sulfur 2p spectra were acquired for each sample using a photon energy of 270 eV. Representative XPS spectra are presented here for each sample. Data points are plotted, along with a fit of the peaks in black and blue respectively. The deconvoluted peaks are presented in brown, green, pink, and blue. The residuals of the fit are plotted at the bottom of each pane.

With the exception of [121]tetramantane-2-thiol on Ag, all monolayers predominantly consist of a single doublet with S $2p_{3/2}$ at about 161.9 eV. This doublet is indicative of silver-thiolate bonding.

[121]tetramantane-2-thiol also shows a doublet with S $2p_{3/2}$ at about 161 eV; this peak is most often attributed to elemental sulfur on the surface. The peak at about 163.5 is attributed to unbound thiol and/or disulfide. The ratio of C 1s to Au $3d_{5/2}$ intensity is a rough measure of thickness: with 500 eV photon energy, this ratio is for **1**: 0.5-0.6, **2**: 1.0-1.2, **3**: 1.5, **4**: 0.8-0.9. For comparison, dodecanethiol is about 3-4.

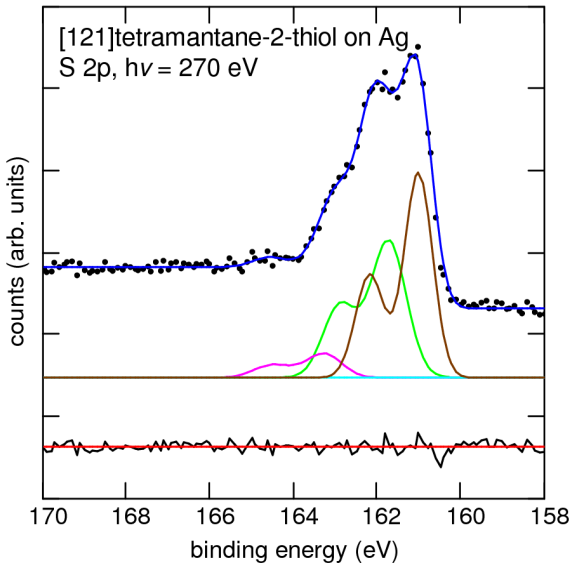

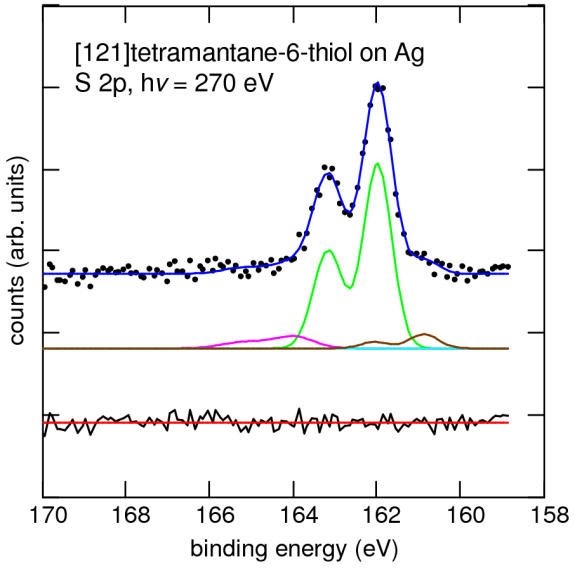

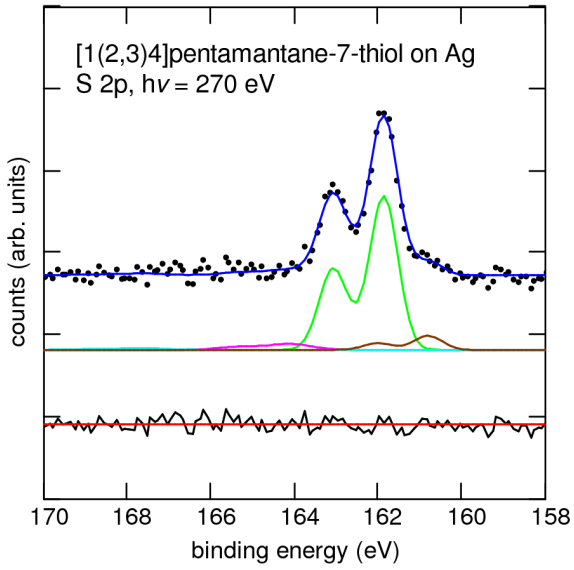

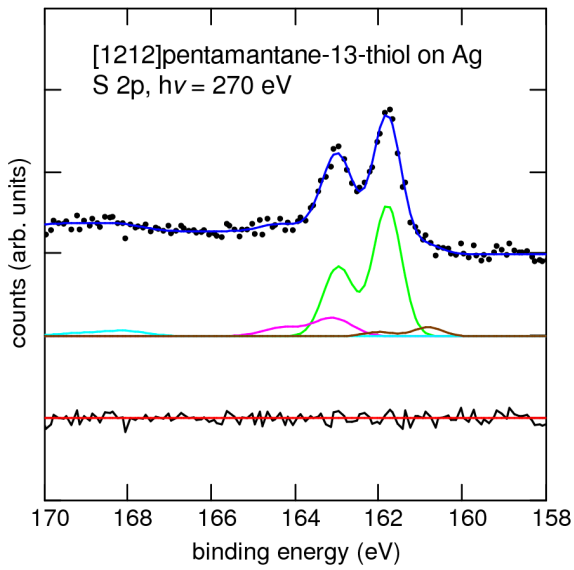

Double Normalization: Obtaining Clean Ag Reference Absorption

Working on silver substrates in TEY mode requires double normalization to not only the upstream gold I_0 grid but a reasonably clean silver substrate, as described in the text. This is easily accomplished by gently heating the silver substrate in UHV to remove the SAM. The sample is heated until the C 1s photoelectron peak is no longer distinguishable from the background, (about 100° C) and then the reference NEXAFS signal from this clean Ag substrate is quickly acquired. At right are XPS spectra from one of our reference substrates during data acquisition; the top pane is the C 1s region. The peak from a dodecanethiol SAM (about twice as thick as our diamondoid SAMs) is shown in black. After heating, the red spectrum reveals carbon contamination at or below the detection limit of the XPS, estimated at less than a few percent. Conversely, in the lower pane, Ag 3d photoelectrons are attenuated by the SAM (black) and are much more prominent after SAM removal (red).